Supplementary Material: Dark state optical lattice with sub-wavelength spatial structure

Y. Wang,[1] S. Subhankar,[1] P. Bienias,[1] M. Łącki,[2,3,4] T-C. Tsui,[1] M. A. Baranov,[3,4] A. V. Gorshkov,[1,5] P. Zoller,[3,4] J. V. Porto,[1] and S. L. Rolston[1]

[1] *Joint Quantum Institute, National Institute of Standards and Technology and the University of Maryland, College Park, Maryland 20742 USA*
[2] *Jagiellonian University, Institute of Physics, Łojasiewicza 11, 30-348 Kraków, Poland*
[3] *Institute for Quantum Optics and Quantum Information of the Austrian Academy of Sciences, A-6020 Innsbruck, Austria*
[4] *Institute for Theoretical Physics, University of Innsbruck, A-6020 Innsbruck, Austria*
[5] *Joint Center for Quantum Information and Computer Science, National Institute of Standards and Technology and the University of Maryland, College Park, Maryland 20742 USA*

(Dated: January 3, 2018)

I. EXPERIMENTAL TECHNIQUES

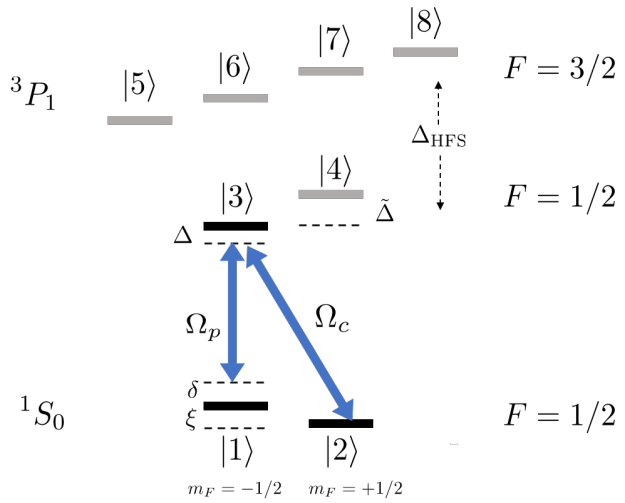

FIG. S1. Level structure of the $^1S_1$ and $^3P_1$ manifolds of ^{171}Yb: δ is the two photon detuning; Δ is the single photon detuning; ξ is the ground state Zeeman splitting and $\tilde{\Delta}$ is the Zeeman splitting in the excited state due to the external magnetic field; and $\Delta_{\rm HFS}$ is the $^3P_1$ hyperfine splitting.

We use forced evaporation of co-trapped ^{87}Rb to sympathetically cool $\sim 3\times10^5$ atoms of ^{171}Yb to a temperature of 1.1 T_F. The ^{87}Rb -^{171}Yb mixture is produced in a combined magnetic and multi-wavelength optical dipole trap [S1]. After reaching the final temperature, the Rb atoms are removed by ramping on the magnetic field to 12 mT. The lifetime of Yb atoms in the trap after removal of the Rb atoms is 3 s. Referring to Fig. 1c. in the main text, the final Yb trap frequencies are $\omega_x \simeq 2\pi \times 164$ Hz, $\omega_{z+y} \simeq 2\pi \times 50$ Hz, and $\omega_{z-y} \simeq 2\pi \times 155$ Hz.

The σ_i^- and π coupling beams at 556 nm are generated from the same laser, which is beat-note (BN) locked to a separate laser (used for laser cooling on the $^1S_0 - {}^3P_1$ transition), which itself is locked to an Yb atomic saturation absorption signal. The dynamic control of the BN allows for rapid tuning of the single-photon detuning Δ of the beams. Separate acousto-optic modulators (AOM) allow for independent intensity control of all three coupling beams, as well as control over the two photon detuning δ and the phase offset between the two σ_i^- beams ($i = 1, 2$) used for shaking the lattice. The three beams are delivered to the atoms through independent optical fibers, and have beam waists of $\sim$ 1mm at the atoms.

We image the atoms using the Yb $^1S_0 - {}^1P_1$ transition at 399 nm, with light generated by a frequency doubled laser system. We stabilize the seed of the imaging laser (at 800 nm) via a scanning transfer cavity lock [S2, S3] with light locked to the $5^2S_{1/2} - 5^2P_{3/2}$ transition at 780 nm in Rb as the reference. State-selectivity is achieved by imaging in a large magnetic field of 12 mT along $\hat{x}$, such that the resulting 116 MHz spacing between the Zeeman states of $^1P_1$ is sufficient to resolve the spin-dependent transitions with linewidth $\Gamma_{1P1} = 2\pi\times30$ MHz. The imaging beam propagates along $\hat{y}$ with linear polarization along $\hat{z}$, such that it has an equal superposition of $\hat{\sigma}_+$ and $\hat{\sigma}_-$ relative to the B-field.

We measure the population in each hyperfine ground state by making the laser resonant with its respective stretched state ($^1S_0\,|F=1/2, m_F=\pm 1/2\rangle \leftrightarrow {}^1P_1\,|F=3/2, m_F=\pm 3/2\rangle$) during imaging.

II. RABI FREQUENCY CALIBRATION

We calibrate the Rabi frequencies of σ_i^- (Ω_{ci}) and π (Ω_p) by measuring two-photon Raman Rabi frequencies and light-shift induced Raman detuning of the $\sigma_i^- - \pi$ pairs of beams as a function of their beam powers. When $\Delta \gg \Gamma, \Omega$, one can adiabatically eliminate the excited state, $|3\rangle$, and reduce the three-level system to an effective two-level system with states $|\vec{p}\rangle\,|1\rangle$ and $\left|\vec{p}+2\hbar\delta\vec{k}\right\rangle|2\rangle$, resulting in the following expressions for the two-photon Rabi frequency (Ω_R) and Raman detuning (δ_R) [S4]

$$\Omega_R = \frac{\Omega_p \Omega_{ci}}{2\Delta} \tag{S1}$$

$$\delta_R = \delta + \frac{4\omega_R(\vec{p}\cdot\delta\vec{k} + \left|\delta\vec{k}\right|)}{\left|\delta\vec{k}\right|} + \xi - \frac{\Omega_{ci}^2}{4\Delta} + \frac{\Omega_p^2}{4\Delta} \tag{S2}$$

where $\delta\vec{k} = \vec{k}_c - \vec{k}_p$, and $\omega_R = \frac{\hbar\left|\delta\vec{k}\right|^2}{2m}$ is the Raman recoil energy. $\vec{k}_c$ and $\vec{k}_p$ are the k-vectors for one of the pump beams and probe beam respectively. For a stationary gas, the second term in (S2) averages to 0.

We extract Ω_R and δ_R by measuring the oscillation of the center of mass (COM) position of the cloud as a function of the Raman pulse time, after a 12 ms time-of-flight (TOF). In addition to transferring population between ground states, stimulated Raman transitions provide a momentum kick i.e. $|\vec{p}\rangle\,|1\rangle \leftrightarrow \left|\vec{p}+2\hbar\delta\vec{k}\right\rangle|2\rangle$. This momentum kick manifests itself in TOF measurements as spatially separated momentum peaks, and the COM position of the cloud provides a measure of the ground state populations. Fig. S2(a) shows typical Rabi oscillation data, which we fit to a damped sinusoid to determine Ω_R. The damping arises from the spread in the momentum distribution of the atoms.

Ω_R gives us information about the product of Ω_{ci} and Ω_p, but not their absolute magnitudes. For fixed Δ, Ω_R and $\delta_R = 0$, Eqs. (S1) and (S2) can be used to determine the two Rabi frequencies Ω_{ci} and Ω_p as a function of laser power. Defining $\Omega_p^2 = A_p P_p$ and replacing $\Omega_{ci} = 2\Omega_R\Delta/\Omega_p$ in Eq. (S2), we get

$$\delta = \xi - \frac{A_p P_p}{4\Delta} + \frac{\Delta\Omega_R^2}{A_p P_p} \tag{S3}$$

where P_p is the power of the probe beam and A_p is the constant that connects Ω_p to P_p.

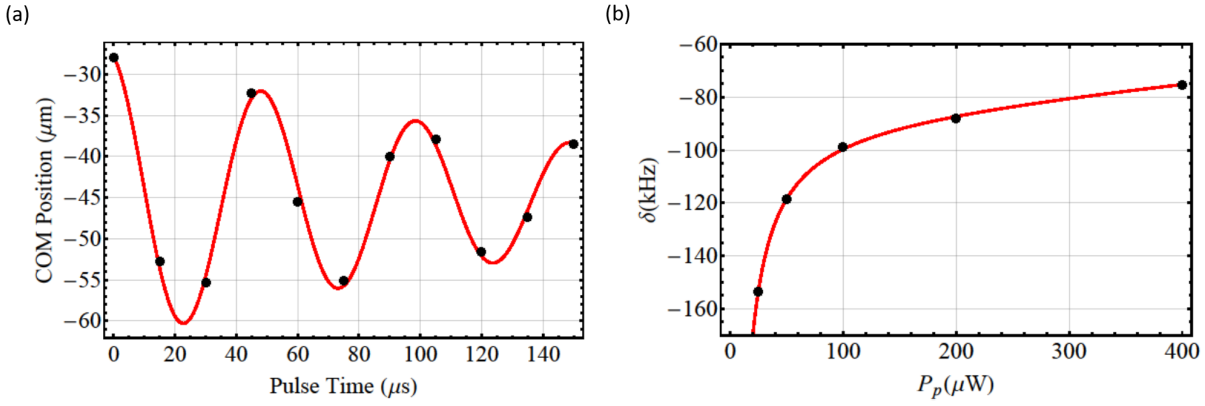

FIG. S2. (a) Example center of mass oscillation of the cloud as a function of Raman pulse time, used to calibrate Rabi frequencies. (b) Change in two-photon detuning (δ) as function of the probe power, P_p.

Experimentally, we fix $\Delta = 40$ MHz and vary P_{ci} (the power of σ_i^- beam) and P_p so as to keep Ω_R constant. We tune δ to satisfy $\delta_R = 0$, determined by maximizing the COM shift after a $\pi/2$ Raman pulse. We fit the measured

values for δ as a function P_p using Eq. (S3) as the fit function with A_p and ξ as fit parameters. Fig. S2(b) shows the fit to data. Defining $\Omega_{ci}^2 = A_{ci}P_{ci}$ just as for the probe beam, we extract A_{ci} using Eq. (S1). Given the uncertainty in the measurement of Ω_R for the two cases, we can determine the balanced condition $\Omega_{c1} = \Omega_{c2}$ to within 2%.

III. IMBALANCED LATTICE BEAMS

To determine the potential $V(x)$ for imbalanced control beams, $\Omega_{c1} \neq \Omega_{c2}$, we consider the spatially dependent control Rabi frequency of the form

$$\Omega_c(x) = \frac{\Omega_{c1}\mathrm{e}^{ikx} - \Omega_{c2}\mathrm{e}^{-ikx}}{i} \tag{S4}$$

When $\Omega_{c1} = \Omega_{c2} = \Omega_c$, we recover $\Omega_c(x) = 2\Omega_c \sin(kx)$. The resulting Hamiltonian in the bare state basis has the form

$$H = \frac{\hbar\Omega_p}{2}\begin{pmatrix} 0 & 0 & 1 \\ 0 & 0 & s\sin(kx) + i\eta\cos(kx) \\ 1 & s\sin(kx) - i\eta\cos(kx) & 0 \end{pmatrix} \tag{S5}$$

where $s = \frac{1}{\epsilon} = \frac{\Omega_{c1}+\Omega_{c2}}{\Omega_p}$ and $\eta = \frac{\Omega_{c1}-\Omega_{c2}}{\Omega_p}$, and $\Delta = \Gamma = \delta = 0$. Diagonalizing H gives the following normalized eigenvectors:

$$|E_0(x)\rangle = -\frac{i\eta\cos(kx) + s\sin(kx)}{\sqrt{(1+\eta^2\cos^2(kx) + s^2\sin^2(kx))}}|1\rangle + \frac{1}{\sqrt{(1+\eta^2\cos^2(kx) + s^2\sin^2(kx))}}|2\rangle$$

$$|E_-(x)\rangle = -\frac{1}{\sqrt{2(1+\eta^2\cos^2(kx) + s^2\sin^2(kx)}}|1\rangle + \frac{(i\eta\cos(kx) - s\sin(kx))}{\sqrt{2(1+\eta^2\cos^2(kx) + s^2\sin^2(kx))}}|2\rangle + \frac{1}{\sqrt{2}}|3\rangle$$

$$|E_+(x)\rangle = \frac{1}{\sqrt{2(1+\eta^2\cos^2(kx) + s^2\sin^2(kx)}}|1\rangle + \frac{(-i\eta\cos(kx) + s\sin(kx))}{\sqrt{2(1+\eta^2\cos^2(kx) + s^2\sin^2(kx))}}|2\rangle + \frac{1}{\sqrt{2}}|3\rangle$$

The resulting scalar potential for the dark state $|E_0(x)\rangle$ [S5] is

$$V(x) = \frac{\hbar^2}{2M}\sum_{j=\pm}|\langle E_j(x)|\nabla|E_0(x)\rangle|^2 = E_R\frac{s^2\cos^2(kx) + \eta^2\sin^2(kx)}{(1+\eta^2\cos^2(kx) + s^2\sin^2(kx))^2} \tag{S6}$$

When there is no imbalance, $\eta = 0$, we recover Eq. (1) from the main text,

$$V(x;\eta=0) = E_R\frac{s^2\cos^2(kx)}{(1+s^2\sin^2(kx))^2} \tag{S7}$$

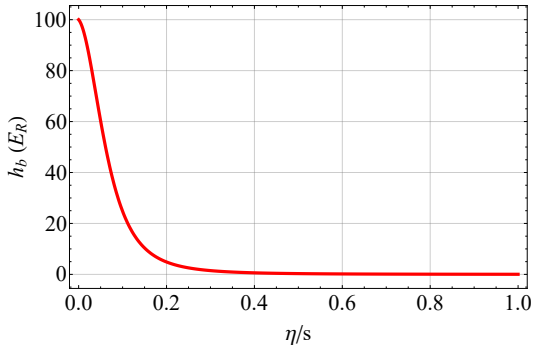

FIG. S3. Growth of the barrier with decrease in η/s.

The barrier height is given by $h_b = V(x=0) = E_R s^2/(1+\eta^2)^2$. In Fig. S3, we show how h_b grows as the imbalance η/s is reduced from 1 to 0 (adiabatically loading into a $100E_R$ lattice). When one of the control beams is turned off, $s^2 = \eta^2$, the potential $V(x)$ is small and spatially homogeneous. Given that our Rabi frequencies $(\Omega_{c1}, \Omega_{c2})$ are balanced to within 2%, the uncertainty in η has negligible effect on the barrier height as $h_b \simeq E_R s^2(1-2\eta^2)$ for $\eta \ll 1$. We also note that the FWHM of the sub-wavelength barriers in the dark state lattice is well approximated by $0.2\lambda\epsilon$ below $\epsilon = 0.3$.

IV. LOADING ATOMS INTO DARK STATE LATTICE AND BANDMAPPING

To adiabatically load atoms into the ground band of the lattice, we first prepare the atoms in $|1\rangle$ by optically pumping using the σ_1^- beam with $\Delta = 12$ MHz. We then change Δ to the final desired value using the BN lock. We ramp on the power of the σ_1^- beam in 0.1 ms and hold for 0.1 ms, followed by ramping on the π beam in 0.3 ms and holding for 0.1 ms. This adiabatically transfers the atoms in $|1\rangle$ into the dark state of the $\sigma_1^- - \pi$ beam configuration. Finally, we ramp on the σ_2^- beam in 1 ms. As discussed in the previous section, this final step ramps the lattice imbalance from $\eta = 1$ to $\eta = 0$, smoothly transforming the potential into the lattice potential.

To find the quasimomentum distribution of the atoms in the dark lattice we perform bandmapping at the end of the experiment by adiabatically ramping down σ_2^- in 0.5 ms (ramping down the barrier height), and then snapping off the σ_1^- beam, the π beam and the optical dipole trap. This maps atoms with given quasimomentum in the lattice to real momentum in free space. We then take an absorption image of this momentum distribution after 12 ms TOF.

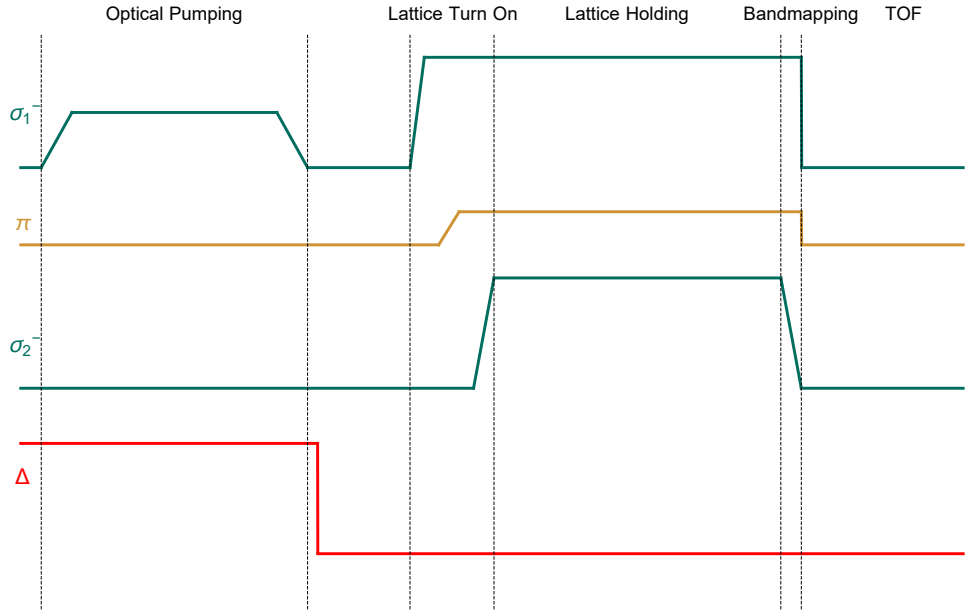

FIG. S4. Procedure to adiabatically load atoms into the ground band of the dark state lattice and performing bandmapping at the end of the sequence.

V. POLARIZATION OPTIMIZATION

The polarization purity of the beams is sensitive to the alignment of the beams, $\vec{k}_p$ and $\vec{k}_{ci}$, with the magnetic field $\vec{B}$. When $\vec{k}_{ci}$ of the circularly polarized control beams is well aligned with $\vec{B}$, the atoms are optically pumped into the trivial dark state, $|1\rangle$. But when the magnetic field is misaligned by an angle θ from $\vec{k}_{ci}$, the resulting π component intensity scales as $\sin^2(\theta)$. The effect of the π component can be investigated in the context of off-resonant EIT. Due to the non-zero ground state Zeeman splitting (89 kHz), the π component and the σ^- component of the control beam are not on two-photon resonance which leads to photon scattering. This causes loss of atoms from the trap. By measuring atom loss as function of the strength of the transverse magnetic field component$(\vec{B}_\perp)$, we adjust $\vec{B}$ such that $\vec{B} \parallel \vec{k}_{c1}$. We then align $\vec{k}_{c2}$ to $\vec{k}_{c1}$ by coupling the σ_2^- beam into the optical fiber that delivers the σ_1^- beam to the atoms with over 50% coupling efficiency.

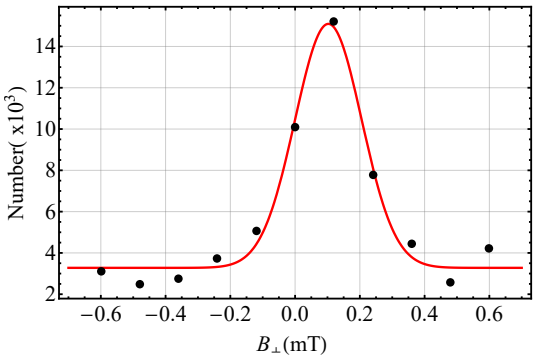

FIG. S5. Atom loss measurement to optimize polarization of σ_1^- beam by scanning the transverse component of magnetic field, $\vec{B}_\perp$.

The polarization of the π beam is optimized by aligning its polarization $\vec{\epsilon_\pi}$ along $\vec{B}$, $\vec{\epsilon_\pi} \times \vec{B} = 0$. This also implies $\vec{k}_p \cdot \vec{B} = 0$ where $\vec{B}$ is the magnetic field that also satisfies $\vec{B} \parallel \vec{k}_{c1}$. We use a Glan-Taylor polarizer to define $\vec{\epsilon}_\pi$. The optimal setting for the polarizer is determined by minimizing loss of atoms from the trap. To satisfy $\vec{k}_p \cdot \vec{B} = 0$, we adjust $\vec{k}_p$ such that the same $\vec{B}_\perp$ satisfies both $\vec{k}_p \cdot \vec{B} = 0$ and $\vec{B} \parallel \vec{k}_{c1}$. We do this via a scheme where we first adjust $\vec{k}_p$ and then perform the measurement we did to make $\vec{B} \parallel \vec{k}_{c1}$ (Fig.S5), but now with the π beam. We iterate this scheme until the $\vec{B}_\perp$ we measure coincides with the $\vec{B}_\perp$ needed to satisfy $\vec{B} \parallel \vec{k}_{c1}$. When the polarization of the π beam is not well aligned with $\vec{B}$, undesired σ component from the π beam causes increased atom loss from the trap. Just as in the case for σ_1^-, this atom loss can be understood in the context of off-resonant EIT. With these techniques, we accurately make $\vec{B} \parallel \vec{k}_{c1}$, $\vec{k}_p \cdot \vec{B} = 0$ and $\vec{\epsilon_\pi} \times \vec{B} = 0$ to within ~ 5 mrad.

VI. LATTICE MODULATION SPECTROSCOPY

We probe the bandstructure of the dark lattice by modulating the phase of the σ_2^- beam with respect to the σ_1^- beam using an analog RF phase-shifter on the RF drive to the AOM for the σ_2^- beam. We transfer atoms from the ground band to the first excited band by shaking the lattice at the appropriate frequency for 200 μs and an amplitude of $\lambda/8$. We then perform bandmapping by ramping down one of the lattice beams in 0.5 ms. We measure the population in each band as a function of modulation frequency and fit a Gaussian to the excited population to extract the transition frequencies.

Since the short lattice shaking pulse is Fourier broadened, we are unable to resolve the quasimomentum dependence of the band excitations when we scan the frequency. We also notice that in order to significantly populate excited bands, a lattice shaking pulse with large amplitude is needed, in contrast to standard sinusoidal lattices where the curvature of band dispersion can be easily resolved with small shaking amplitudes and longer pulse times. In standard sinusoidal optical lattices, the Rabi frequency between a pair of bands is proportional to the shaking amplitude and the lattice depth, and a small shaking amplitude in deep lattices can significantly populate the excited bands. This is in contrast with the KP lattice, where the Rabi frequency is proportional to shaking amplitude, but independent of the barrier height. Larger shaking amplitudes are required to transfer substantial population to the excited bands. In addition, since the wavefunction in the dark state lattice goes to zero at the barriers and the potential is flat elsewhere (where most of the wavefunction lives), the barrier excursion during a lattice shaking pulse needs to be large to diabatically distort the wavefunction between the barriers and hence cause band excitations.

In Figs. 3(a) and 3(b) of the main text, we note that the frequencies of the transitions ($s \to p$ and $s \to p \to d$) measured are slightly lower than the shaded regions. The dipole nature of the coupling due to lattice shaking allows only transitions between bands of opposite parity i.e. $s \leftrightarrow p$ and $p \leftrightarrow d$. The population in the d band arises after some population has been transferred into the p band from the s band, which may affect the resonance spectrum. To better understand this potential systematic redshift of the measured transition frequencies, we employ a model where we map the first three bands (s, p, d) of the dark-lattice to an ensemble of discrete three-level ladder-type systems where the energy spacings trace the curvatures of the bands sampled at various values of q. We solve the full time-dependent Hamiltonian with an appropriate scaling factor for the drive strength and fit the ensemble average of the population in the excited states as a function of lattice shaking frequency to estimate the transition frequencies. These estimated transition frequencies are systematically lower by $\sim E_R/3$ than the average transition frequency between the bands

which, has the same sign as the redshifts observed but is too small to account for all of the shift.

VII. MULTI-LEVEL MODEL

Fig. S1 depicts the three hyperfine states that constitute the Λ-system consisting of $|1\rangle, |2\rangle$, and $|3\rangle$ (black) along with five hyperfine states (grey) that the Λ system is coupled to off-resonantly. Couplings to these off-resonant states affect the bandstructure of the Λ-system. We account for the effect of these off-resonant couplings by adiabatically eliminating the five far off-resonant hyperfine states, which to second ordeer shifts the energies of the ground states of the Λ-system, $|1\rangle$ and $|2\rangle$, by $\delta_1(x)$ and $\delta_2(x)$ respectively.

The Hamiltonian for our effective Λ-system is as follows.

$$H = -\frac{\hbar^2\partial_x^2}{2m} + \hbar \begin{pmatrix} \delta_1(x) & 0 & \frac{\Omega_p}{2} \\ 0 & \delta_2(x) & \frac{\Omega_c(x)}{2} \\ \frac{\Omega_p}{2} & \frac{\Omega_c(x)}{2} & -(\Delta + i\frac{\Gamma}{2}) \end{pmatrix} \tag{S8}$$

Here we use the same treatment to solve this non-hermitian Hamiltonian, as explained in [S6]. As H has the periodicity of λ, we use Bloch's theorem to define the wavefunction that solves H as $\vec{\Phi}(x) = (u_1(x), u_2(x), u_3(x))^T$, where $u_j(x) = \sum_{n=-N}^{n=N} C_{j,q,n} e^{i(q+\frac{2n\pi}{\lambda})x}$ for $j = 1, 2, 3$. Here $u_1(x), u_2(x)$, and $u_3(x)$ represent the atomic wavefunctions for states $|1\rangle, |2\rangle$ and $|3\rangle$ respectively, and q is the quasimomentum such that $q \in [-\pi/\lambda, \pi/\lambda]$. The basis truncation at N must be chosen large enough to correctly capture the non-adiabatic couplings between bright and dark Born-Oppenheimer states at high momenta, and for the typical values of the parameters used in the experiment (e.g. $\Omega_p = 5 - 30\Gamma$, $\Omega_c = 70 - 100\Gamma$, and $\Delta = 2\pi \times 4$MHz), we find $N = 105$ to be sufficient to simulate the bandstructure.

The expressions for the ac-Stark shifts, $\delta_1(x)$ and $\delta_2(x)$, due to off-resonant Rabi couplings are as follows.

$$\delta_1(x) = \delta - \frac{\Omega_p^2}{2\Delta_{\text{HFS}}} - \frac{3\Omega_c(x)^2}{8\Delta_{\text{HFS}}} \tag{S9}$$

$$\delta_2(x) = -\frac{\Omega_p^2}{4\tilde{\Delta}} - \frac{\Omega_p^2}{2\Delta_{\text{HFS}}} - \frac{\Omega_c(x)^2}{8\Delta_{\text{HFS}}} \tag{S10}$$

Substituting the expressions for $\delta_1(x)$ and $\delta_2(x)$ in Eq. (S8) and using the Bloch ansatz we calculate the bandstructure for the Λ system.

The effects of the off-resonant couplings on the dark state ($|E_0(x)\rangle$) can also be understood in the context of perturbation theory. With the perturbing Hamiltonian given by

$$H_{\text{pert.}} = \hbar \begin{pmatrix} \delta_1(x) & 0 & 0 \\ 0 & \delta_2(x) & 0 \\ 0 & 0 & 0 \end{pmatrix} \tag{S11}$$

the first order correction to $V(x)$ is:

$$V_{\text{pert.}}(x) = \langle E_0(x)| H_{\text{pert.}} |E_0(x)\rangle = \hbar \left(\frac{\delta_2 \Omega_p^2}{\Omega_p^2 + \Omega_c^2(x)} + \frac{\delta_1 \Omega_c^2(x)}{\Omega_c^2(x) + \Omega_p^2} \right) \tag{S12}$$

where $|E_0(x)\rangle = \frac{-\Omega_c(x)|1\rangle + \Omega_p|2\rangle}{\sqrt{\Omega_c^2(x) + \Omega_p^2}}$. With independent control over the two-photon detuning (δ), we are able to engineer sub-wavelength traps as depicted in the upper panel of Fig. 3(b) in the main text.

We also note an interesting feature upon simulating the bandstructure for various values of ϵ. As ϵ is decreased from 0.2 to 0.05, we observe that the curvature of the band inverts as shown in Fig. S6. For reference, we also present the bandstructure calculated for just the potential $H = \frac{p^2}{2m} + V(x) + V_{\text{pert.}}(x)$ for each ϵ, represented as black dashed lines. At a particular value of ϵ, which in this case is $\simeq 0.125$, the bandwidth vanishes due to destructive interference between the normal hopping within dark state and the upper bright state assisted hopping implying no tunneling despite barriers having finite width and height.

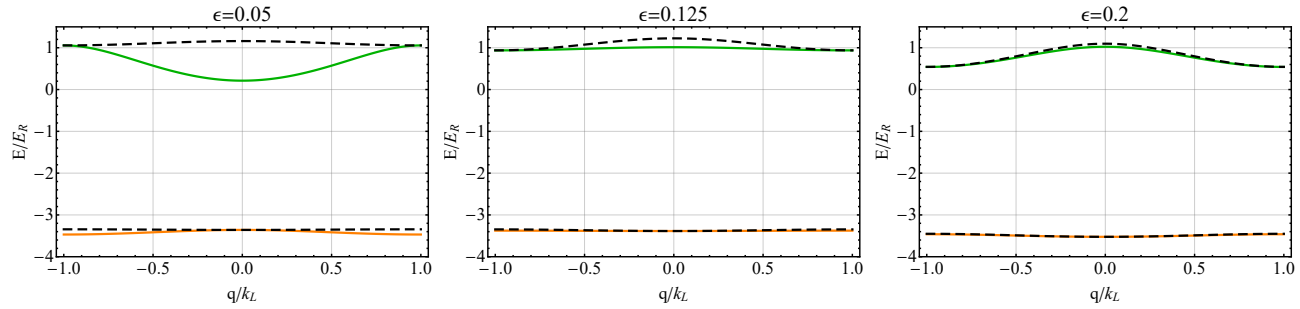

FIG. S6. Change in curvatures of the first two bands of the dark state lattice for different ϵ. Colored lines represent bands for the H given by Eq. (S8) and black dashed lines represent bands for $H = \frac{p^2}{2m} + V(x) + V_{\text{pert.}}(x)$.

VIII. ESTIMATE OF LOSSES BASED ON TRANSMISSION THROUGH A SINGLE BARRIER

In this section, we provide estimates of losses present in our system, based on the analysis of scattering from a single barrier created by $\Omega_c = \Omega_p x/w$, where $w = \epsilon\lambda/(2\pi)$ [S7]. The advantage of this approach is that we can analytically calculate P_{NA}, the probability to lose an atom into state $|E_-\rangle$ from state $|E_0\rangle$ due to non-adiabatic coupling between the states, as well as provide intuitive explanations for P_{sc}, the probability of scattering a photon from state $|3\rangle$. This approach is discussed in Ref. [S7], where P_{NA} and P_{sc} are calculated for $\Delta = 0$. An alternative complementary approach for the estimation of losses is discussed in section IX.

First, we estimate P_{sc} for the case when the detuning $\Delta = 0$. We follow the physical argument from Ref. [S7] to estimate the probability P_e of being in the excited state $|3\rangle$: the dark state probability at $x = 0$ is $\sim |t|^2 \sim E/E_w$, where $E_w = \hbar^2/(2mw^2)$ is the barrier height as well as the strength of the non-adiabatic coupling. The admixture of $|E_-\rangle$ and $|E_+\rangle$ (and hence of $|3\rangle$) is simply $\sim (E_w/(\Omega_p/2))^2$, where E_w plays the role of an effective Rabi frequency and $\Omega_p/2$ plays the role of detuning. Multiplying the two together we obtain $P_e \sim \frac{4EE_w}{\Omega_p^2}$. Then the probability of scattering a photon in a single pass is $P_{\text{sc}} \sim \Gamma P_e 2w/v$, where $2w/v$ is the approximate crossing time for atoms having velocity $v = \sqrt{2E/m}$. In order to estimate the impact of these losses on dark-state lifetime in the lattice, we multiply P_{sc} by the rate $R_{\lambda/2} = v/(\lambda/2)$ with which atoms scatter from the barriers separated by $\lambda/2$. This leads to photon scattering rate $\gamma_{\text{sc}} = c_{\text{sc}} P_{\text{sc}} R_{\lambda/2}$, where the prefactor c_{sc} is on the order of unity. We have confirmed the validity of this expression by numerically calculating the photon scattering rate γ_{sc} from a single barrier as

$$\gamma_{\text{sc}} = \Gamma \frac{\int_{-2w}^{2w} |\psi_e(x)|^2}{\int_0^{\lambda/2} |\psi_{E_0}(x)|^2}, \tag{S13}$$

where $\psi_e(x)$ and $\psi_{E_0}(x)$ are the amplitudes to be in states $|3\rangle$ and $|E_0\rangle$, respectively, for and incoming dark-state plan wave. From comparison with numerical results, we find that the prefactor c_{sc} is approximately 0.9. The second imperfection comes from the nonzero probability P_{NA} of losing the atom into the open $|E_-\rangle$ channel due to the nonadiabatic coupling between $|E_0\rangle$ and $|E_-\rangle$. Based on Ref. [S7], we know that $P_{\text{NA}} \approx 1.37\sqrt{E/E_w} e^{-1.75\sqrt{\Omega_p/(2E_w)}}$. In order to estimate the impact of these losses on dark-state lifetime in the lattice, we multiply P_{NA} by the rate $R_{\lambda/2}$, which leads to the rate $\gamma_{\text{NA}} = 2P_{\text{NA}}\sqrt{2E/m}/\lambda$ of losing atoms into state $|E_-\rangle$.

Using the expressions for γ_{sc} and γ_{NA} found above, we can estimate the decay rate γ_n of the n-th Bloch band dark state by evaluating $\gamma_{\text{sc}} + \gamma_{\text{NA}}$ at $E = E_n$. In order to test the relation between our barrier-based results and the results from a direct lattice calculation more quantitatively, we consider $\gamma_1 = \gamma_{1,\text{sc}} + \gamma_{1,\text{NA}}$ for the lowest Bloch band (subscript 1 indicates the number of the band) for the parameters as in Fig. 3(left) from the supplement of Ref. [S6]. We find good agreement between the lattice-based calculation and the barrier-based calculation, see Fig. S7. Moreover, we see that $\gamma_{1,\text{NA}}$ is much smaller than $\gamma_{1,\text{sc}}$ for the parameters considered; therefore the scaling with Ω_p is given by the scaling of $\gamma_{1,\text{sc}}$. Since, for fixed n, all terms except P_e are Ω_p-independent, the scaling of γ_1 with Ω_p is governed by the scaling of P_e with Ω_p. This gives us a physical explanation for the numerically observed scaling in Fig. 3(left) in the supplement of Ref. [S6], as well as for the scaling of our experimental results, which we comment on below.

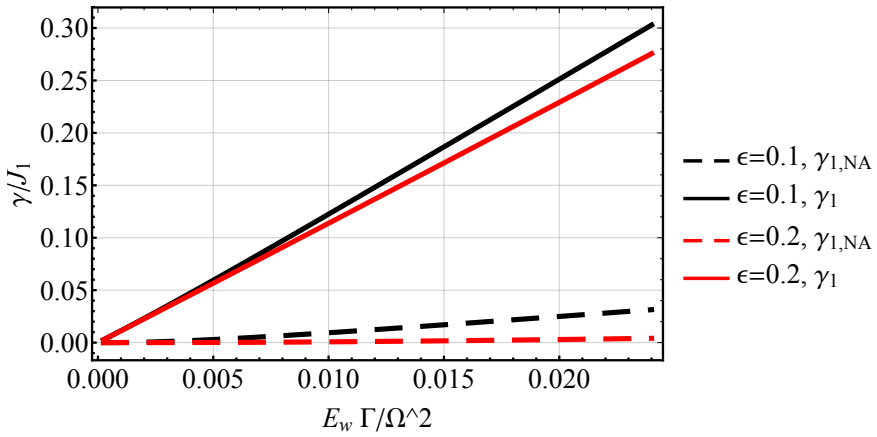

FIG. S7. We plot analytical results for the total decay rate $\gamma_1 = \gamma_{1,\mathrm{NA}} + \gamma_{1,\mathrm{sc}}$ and the non-adiabatic decay rate $\gamma_{1,\mathrm{NA}}$ for the first Bloch band in units of $J_1 = 2\epsilon E_R/\pi^2$ as a function of $E_w\Gamma/\Omega_p^2$ for $\Delta = 0$, $\Gamma = 600E_R$, and two different values of ϵ. Note that the prefactor c_{sc} is fixed using the numerics for a single barrier. For comparison with analogous results for a direct lattice calculation, see Fig. 3(left) in the Supplementary materials for Ref. [S6]. The numerics for a barrier gives the decay rate γ_1 approximately two times greater than the decay from lattice calculations. Note that, for $\epsilon = 0.1$, losses due to P_{NA} become non-negligible.

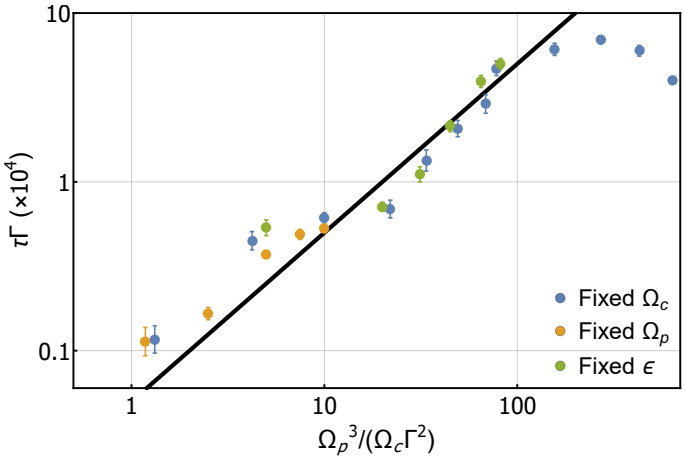

FIG. S8. Lifetime plotted on a log-log scale against the parameter $\Omega_p^3/(\Omega_c\Gamma^2)$ under three conditions: keep $\Omega_c = 100\Gamma$ and scan Ω_p from 5 to 40 Γ (blue); keep $\Omega_p = 5\Gamma$ and scan Ω_c from 12.5 to 100 Γ (orange); and keep $\epsilon = 0.2$ fixed and scan Ω_p from 2.5 to 20 Γ (green). A linear fit $\tau\Gamma \propto \Omega_p^3/(\Omega_c\Gamma^2)$ is also shown (black line).

In Fig. S8, we plot the experimentally observed lifetime as a function of the parameter $\Omega_p^3/(\Omega_c\Gamma^2)$ for different cases where we vary ϵ, Ω_p, and Ω_c. We checked based on barrier numerics for the complete data set that τ has a greater or equal contribution from γ_{sc} than from γ_{NA}. This explains the observed linear scaling over orders of magnitudes of $\tau\Gamma$ with $\Omega_p^3/(\Omega_c\Gamma^2)$. This linear scaling is plotted as a black line in Fig. S8.

Finally, we comment on the dependence of $\gamma_{\mathrm{sc}} + \gamma_{\mathrm{NA}}$ on Δ. In this case, both P_{sc} and P_{NA} are relevant, and the interplay between them describes the results shown in Fig. 4(a) in the main text. For $\Delta < 0$, P_{NA} gives a leading contribution to τ, whereas, for $\Delta > 0$, P_{NA} is negligible and the leading contribution comes from P_{sc}. P_{NA} strongly depends on Δ, whereas P_{sc} is only very weakly dependent on Δ. This explains the observed asymmetry in the dependence of losses on Δ, as explained in the main text. Finally, we numerically confirmed that the results (not shown) based on barrier calculations describe well the quantitative behavior of the losses as a function of Δ and quantitatively agree with the full lattice calculations. The full lattice analysis is presented in the next section.

IX. THEORY FOR LIFETIME MEASUREMENTS BASED ON PERTURBATIONS TO THE DARK STATE

Here we use a direct lattice-based calculation to explain the lifetime in the context of perturbations to the dark state eigenfunction induced by couplings to the bright channels and off-resonant couplings to states outside the Λ-system (Fig. S1). The imaginary part of the dark state eigenenergy determines the scattering rate of the atoms which determine their lifetime in the trap up to a scaling factor. The couplings between the dark and bright channels are small when the energy separations between them are large. As we change Δ, Ω_p, and Ω_c, we alter the admixture of $|3\rangle$ into the dark state and hence the amount of photon scattering. First we discuss the measured lifetime in the context of two beam EIT (inset of Fig. 4(a) in the main text) and then explain the lifetime measurements in the dark state lattice when we scan Δ and Rabi frequencies Ω_p and Ω_c (Fig. 4(a) and Fig. 4(b) in the main text).

When the off-resonant couplings to the Λ-system are neglected the Hamiltonian is given by:

$$H = -\frac{\hbar^2}{2m}\left(\frac{\partial^2}{\partial x^2}+\frac{\partial^2}{\partial y^2}+\frac{\partial^2}{\partial z^2}\right)+\hbar\begin{pmatrix} 0 & 0 & \Omega_p e^{iky}/2 \\ 0 & 0 & \Omega_c(x)/2 \\ \Omega_p e^{-iky}/2 & \Omega_c^*(x)/2 & -\Delta' \end{pmatrix} \tag{S14}$$

with $\Delta' = \Delta + \frac{i\Gamma}{2}$. In the experiment $\Omega_c(x)$ can be either $\Omega_c(x) = \Omega_c e^{ikx}$ with lasers in the homogeneous EIT configuration, or $\Omega_c(x) = \Omega_c \sin kx$ for standing wave case.

A. Homogenous EIT configuration

We first consider the two-beam EIT configuration. In this configuration the non-hermitian Hamiltonian (S14) can be exactly diagonalized by finding a proper biorthogonal basis. The right eigenvectors are indexed by the 3D momentum $\vec{q}$, and are of the form:

$$e^{i\vec{q}\cdot\vec{r}}(ae^{iky}|1\rangle + be^{ikx}|2\rangle + c|3\rangle) \tag{S15}$$

where $(a,b,c)^\dagger$ is a right eigenvector of the matrix:

$$H_{\vec{q},k} = \begin{pmatrix} \frac{\hbar^2}{2m}(q^2+2kq_y+k^2) & 0 & \hbar\Omega_p/2 \\ 0 & \frac{\hbar^2}{2m}(q^2+2kq_x+k^2) & \hbar\Omega_c/2 \\ \hbar\Omega_p/2 & \hbar\Omega_c/2 & -\hbar\Delta'+\frac{\hbar^2 q^2}{2m} \end{pmatrix} \tag{S16}$$

with $q^2 = q_x^2+q_y^2+q_z^2$.

The Hamiltonian $H_{\vec{q},k}$ can be diagonalized analytically, however the resulting expressions are complicated. For the experimental parameters, both $\hbar^2q^2/2m$ and the recoil energy $\hbar^2k^2/2m$ are much smaller than $\hbar\Omega_c$ and $\hbar\Omega_p$, defining small parameters with respect to which one can expand. Expanding up to the second order we get the following expression for the energy of the dark state:

$$E_0 \approx \frac{\hbar^2q^2}{2m}+\frac{\hbar^2}{2m}\left(k^2+\frac{2kq_y\Omega_c^2}{\Omega_c^2+\Omega_p^2}+\frac{2kq_x\Omega_p^2}{\Omega_c^2+\Omega_p^2}\right)-\left(\frac{\hbar^3}{m^2}\right)\frac{4\Delta\Omega_c^2\Omega_p^2k^2\left(q_y-q_x\right)^2}{\left(\Omega_c^2+\Omega_p^2\right)^3}-\left(\frac{\hbar^3}{m^2}\right)\frac{2i\Gamma\Omega_c^2\Omega_p^2k^2\left(q_y-q_x\right)^2}{\left(\Omega_c^2+\Omega_p^2\right)^3}, \tag{S17}$$

with imaginary part $\mathrm{Im}E_0$ Δ-independent. The last two terms in (S17) appear then as a second order correction. It should be mentioned that the imaginary term in Eq. (S17) is a sum of Δ-dependent contributions from the upper and from the lower bright states. In their sum, however, the Δ-dependence disappears.

The other loss mechanism results from off-resonant couplings to the states beyond the Λ-system ($|4\rangle, |5\rangle, |6\rangle$, and $|7\rangle$ in Fig. S1). This additional loss rate is given by

$$\Gamma_{\text{offres.}} = \Gamma\frac{\Omega_p^4}{4\tilde{\Delta}^2\left(\Omega_c^2+\Omega_p^2\right)}+\Gamma\frac{5\Omega_c^2\Omega_p^2+3\Omega_c^4+4\Omega_p^4}{8\Delta_{\text{HFS}}^2\left(\Omega_c^2+\Omega_p^2\right)}, \tag{S18}$$

and is approximately Δ-independent. For the parameters used in the experiment for the EIT configuration we find $\Gamma_{\text{offres.}}$ to be approximately a factor of two smaller than the loss rate from Eq. (S17). We conclude that the combined loss rate in the homogeneous EIT configuration is approximately Δ-independent, in agreement with the results shown in the inset of Fig. 4(a).

B. Standing wave case

We now consider the standing-wave case. In contrast to the homogeneous EIT configuration, the standing wave case does not admit an exact analytic treatment. Although the Hamiltonian (S14) can be diagonalized numerically, to support our numerical results and to get an insight into underlying loss mechanisms, we present below the analysis based on the Born-Oppenheimer (BO) approach (as in Ref. [S6]).

We first diagonalize the atomic part of the non-Hermitian Hamiltonian (S14) (the last term) to find its BO eigenstates: The dark state right eigenvector

$$|E_0(y,x)\rangle = \frac{1}{N_0}\left[(-\Omega_p)\,|2\rangle + \Omega_c(x)e^{iky}|1\rangle\right], \quad N_0 = \sqrt{\Omega_c^2(x)+\Omega_p^2}$$

and the two bright states

$$|E_\pm(y,x)\rangle = \frac{1}{N_\pm}\left[\Omega_c(x)|2\rangle + \left(\Delta' \pm \sqrt{\Omega_c^2(x)+\Omega_p^2+\Delta'^2}\right)|3\rangle + \Omega_p e^{iky}|1\rangle\right],$$

where $N_\pm = \sqrt{2}\sqrt{\Omega_c^2(x)+\Omega_p^2+\Delta'\left(\Delta' \mp \sqrt{\Omega_c^2(x)+\Omega_p^2+\Delta'^2}\right)}$.

The eigenfunctions of the Hamiltonian (S14) can be written as

$$\psi(x,y,z) = e^{iq_z z + iq_y y}\left(f_0(x)|E_0(y,x)\rangle + f_+(x)|E_+(y,x)\rangle + f_-(x)|E_-(y,x)\rangle\right),$$

and the Hamiltonian for the wave functions $f_0(x)$ and $f_\pm(x)$ in the BO basis takes the form (see Ref. [S6])

$$\begin{aligned}
\mathcal{H} = &-\frac{\hbar^2\partial_x^2}{2m} + \frac{\hbar^2 q_y^2}{2m} + \frac{\hbar^2 q_z^2}{2m} + \begin{pmatrix} 0 & 0 & 0 \\ 0 & E_+ & 0 \\ 0 & 0 & E_- \end{pmatrix} \\
&+\frac{\hbar^2}{2m}\frac{\Omega_c'^2(x)\Omega_p^2}{\left(\Omega_c^2(x)+\Omega_p^2\right)^2}\begin{pmatrix} 1 & 0 & 0 \\ 0 & M_+^2+C^2 & 0 \\ 0 & 0 & M_-^2+C^2 \end{pmatrix} \\
&-\frac{i\hbar}{2m}\left(\partial_x\hat{A} + \hat{A}\partial_x\right) \\
&-\frac{\hbar^2}{2m}\frac{\Omega_c'^2(x)\Omega_p^2}{\left(\Omega_c^2(x)+\Omega_p^2\right)^2}\begin{pmatrix} 0 & CM_- & -CM_+ \\ CM_- & 0 & -M_+M_- \\ -CM_+ & -M_+M_- & 0 \end{pmatrix} \\
&+\frac{\hbar^2}{2m}\begin{pmatrix} D_{00} & D_{0-} & D_{0+} \\ D_{0-} & D_{--} & D_{+-} \\ D_{0+} & D_{-+} & D_{++} \end{pmatrix},
\end{aligned} \tag{S19}$$

where

$$E_\pm = \frac{1}{2}\left(-\Delta' \pm \sqrt{\Omega_c^2(x)+\Omega_p^2+\Delta'^2}\right) \tag{S20}$$

and the matrix $\hat{A}$ has the form

$$\hat{A} = -i\hbar\frac{\Omega_c'(x)\Omega_p}{\Omega_c^2(x)+\Omega_p^2}\begin{pmatrix} 0 & -M_+ & -M_- \\ M_+ & 0 & -C \\ M_- & C & 0 \end{pmatrix}.$$

The coefficients

$$C = \Delta'\frac{\Omega_c(x)}{2\Omega_p}\frac{\Omega_c^2(x)+\Omega_p^2}{\Omega_c^2(x)+\Omega_p^2+\Delta'^2}$$

and

$$M_\pm = \left[1 + \frac{2E_\pm(x)}{\Omega_c^2(x) + \Omega_p^2}\right]^{-1/2}.$$

determine couplings between the dark and the bright state manifold, which takes place in the region of subwavelength peaks. They also result in the energy corrections to the bright states [second line, Eq (S19)], which are typically much smaller than $E_\pm$. The matrix in the last line of (S19) originates from the y-dependent phase of Ω_p and has elements

$$D_{00} = \frac{\Omega_c^2(x)k(k+2q_y)}{N_0^2},$$

$$D_{0\pm} = \frac{\Omega_c(x)\Omega_p k(k+2q_y)}{N_0 N_\pm},$$

$$D_{\pm\pm} = \frac{\Omega_p^2 k(k+2q_y)}{N_\pm^2},$$

$$D_{\mp\pm} = \frac{\Omega_p^2 k(k+2q_y)}{N_\pm N_\mp}.$$

Note that D_{00} gives a correction to the dark state non-adiabatic potential, Eq. (1) in the main text, which is small under the conditions of the experiment.

Considering the first two terms in (S19) as a zero-order Hamiltonian (where the dark- and bright state BO channels are decoupled), we define the dark state eigenfunctions $\psi^{E_0}_{(\vec{q},n)}(x,y,z)$ and bright states ones $\psi^{E_\pm}_{(\vec{q},n)}(x,y,z)$, where q_z and q_y are the transverse momenta, $q_x \in [-\pi/\lambda, \pi/\lambda]$ is the lattice quasimomentum, and n being the band index. The corresponding energies are $E_{0,(\vec{q},n)}$ and (complex) $E_{\pm,(\vec{q},n)}$, respectively. Note that q_x, q_y, and q_z are conserved quantum numbers even when the couplings between the BO channels are taken into account, in contrary to n.

We can now consider the couplings between the BO channels [other terms in the Hamiltonian (S19)] perturbatively assuming the gaps between the BO states being much larger than the coupling matrix elements. The finite lifetime of the dark state $\psi^{E_0}_{(\vec{q},n)}$ is given by the imaginary part of the corresponding eigenenergy, which appears in the second order contribution

$$\delta^{(2)}E_{0,(\vec{q},n)} = \sum_{\sigma=\pm}\sum_m \frac{{}_L\langle\psi^{E_0}_{(\vec{q},n)}|\mathcal{H}|\psi^{E_\sigma}_{(\vec{q},m)}\rangle_R\, {}_L\langle\psi^{E_\sigma}_{(\vec{q},m)}|\mathcal{H}|\psi^{E_0}_{(\vec{q},n)}\rangle_R}{E_{0,(\vec{q},n)} - E_{\sigma,(\vec{q},m)}}. \tag{S21}$$

To analyze the Δ-dependence of the imaginary part of $\delta^{(2)}E_{0,(\vec{q},n)}$, we first notice that the largest contributions to the matrix elements $\langle\psi^{E_\sigma}_{(\vec{q},m)}|\mathcal{H}|\psi^{E_0}_{(\vec{q},n)}\rangle$ from the spacial integrals come from the states with eigenenergies close to $\min \mathrm{Re}\epsilon_+$ for the upper bright states, and close to $\max \mathrm{Re}\epsilon_-$for the lower ones. Matrix elements with other states are small because their spatial wave functions are either rapidly oscillating or exponentially suppressed in the coupling regions.

In the red detuned case $\Delta < 0$, the upper bright states are pushed away from the dark ones. This leads to the decrease of the coupling matrix elements with the relevant states because the amplitudes of the internal states $|1\rangle$ and $|2\rangle$ in the upper bright state decrease in favor of $|3\rangle$. On the other hand, the relevant lower bright states are pushed towards the dark ones, with increasing amplitudes of $|1\rangle$ and $|2\rangle$ in its internal structure. In the experiment we have $|\Delta| \lessapprox \Omega_c$ and, as a result, Im $E_{-,\vec{q},n}$ remains approximately unchanged and close to $-\Gamma/4$ for the states close to $\max \mathrm{Re}\epsilon_-$. Therefore, the dominant contribution to $\mathrm{Im}\delta^{(2)}E_{0,(\vec{q},n)}$ comes from the lower bright states and increases with $|\Delta|$, resulting in the decrease of the life-time observed in the experiment, see Fig. 4(a).

In the opposite case $\Delta > 0$, the contribution of the lower dark states decreases, while the contribution of the upper bright states increases and becomes dominant. Here, however, the decrease of imaginary part of $E_{+,(\vec{q},m)}$ dominates over the growth of its real part and over weak increase of the coupling matrix elements, such that $\mathrm{Im}\delta^{(2)}E_{0,(\vec{q},n)}$ decreases with increasing Δ in agreement with the experimental observations.

Finally, we mention that the life-time is an increasing function of Rabi frequencies Ω_c, Ω_p, see Fig. 4(b). This is due to the increase of the gaps to the bright states, while the couplings matrix elements remain practically unchanged.

Connecting Eq. (S21) to the population decay rate is done in the following way: we assume a homogeneous trapped gas with a Fermi-Dirac distribution, where the chemical potential is chosen to fit the total number of particles. For each band index n and quasimomentum $\vec{q}$ the decay rate $\Gamma_{(\vec{q},n)}$ is evaluated by finding the imaginary part of the eigenenergy in Eq. (S21). Since most of the atoms occupy the lowest band of the lattice, we average $\Gamma_{(\vec{q},n)}$ over the lowest three bands to find the average decay rate, which is justified by the fact that the third band almost gives no contribution ($<5\%$). We use the experimentally measured atom number, temperature, and trapping frequencies as the inputs for each data point of Fig. 4, which explains why the theory curve is not smooth in Fig. 4.

[S1] V. D. Vaidya, J. Tiamsuphat, S. L. Rolston, and J. V. Porto, Phys. Rev. A **92**, 043604 (2015).

[S2] S. Subhankar, Y. Wang, A. Restelli, S. L. Rolston, and J. V. Porto, (2018), in preparation.

[S3] J. H. T. Burke, O. Garcia, K. J. Hughes, B. Livedalen, and C. A. Sackett, Review of Scientific Instruments **76**, 11 (2005).

[S4] D. Steck, "Quantum and Atom Optics", available online at http://steck.us/teaching.

[S5] M. Cheneau, S. P. Rath, T. Yefsah, K. J. Günter, G. Juzeliūnas, and J. Dalibard, EPL (Europhysics Letters) **83**, 60001 (2008).

[S6] M. Łącki, M. A. Baranov, H. Pichler, and P. Zoller, Phys. Rev. Lett. **117**, 233001 (2016).

[S7] F. Jendrzejewski, S. Eckel, T. G. Tiecke, G. Juzeliūnas, G. K. Campbell, L. Jiang, and A. V. Gorshkov, Phys. Rev. A **94**, 063422 (2016).